Supplementary Materials for

Diversity of Viscoelastic Properties of an Engineered Muscle-Inspired Protein Hydrogel

Anders Aufderhorst-Roberts, Sophie Cussons, David J. Brockwell, Lorna Dougan*

*Corresponding author. Email: l.dougan@leeds.ac.uk

Supplementary Text

Analysis of Polyprotein Dimensions

The polyprotein structure comprises a concatenated series of five *I*27 protein domains as shown in figure S1. Linkers comprising 4-6 amino acids were inserted between domains to decrease inter-domain interactions. A hexahistidine tag is found at the N-terminus and a dicysteine group is found at the C-terminus.

Dimensions and distances are determined using the 'distance' tool in the molecular visualization software PyMOL. The individual *I*27 domains each have an N-C end-to-end length of l_{domain} = 4.66 nm. Each of the four linker domains contain between 4-6 amino acids with no intrinsic secondary structure. Given that the average linker length is 5 residues, that the average length of an amino acid is 0.35 nm, and assuming that the linker adopts a freely-jointed-chain structure, the total average length of the linker l_{link} is: l_{link} =0.35 nm$\times\sqrt{5}$ =0.78 nm.

From this we may estimate the following:

1. The mean distance between tyrosine crosslink sites is $l_{domain} + l_{link}$ =5.44 nm
2. The ratio between the linker length and polyprotein radius as $\frac{2l_{link}}{l_{domain}} = 0.34$.

b

```
   1  MHHHHHHSSL IEVEKPIYGV EVFVGETAHF EIELSEPDVH GQWKLKGQPL
  51  TASPDSEIIE DGKKHILILH NSQLGMTGEV SFQAANAKSA ANLKVKELVE
 101  ARLIEVEKPL YGVEVFVGET AHFEIELSEP DVHGQWKLKG QPLTASPDSE
 151  IIEDGKKHIL ILHNSQLGMT GEVSFQAANA KSAANLKVKE LLIEARLIEV
 201  EKPIYGVEVF VGETAHFEIE LSEPDVHGQW KLKGQPLTAS PDSEIIEDGK
 251  KHILILHNSQ LGMTGEVSFQ AANAKSAANL KVKELLSSAR LIEVEKPIYG
 301  VEVFVGETAH FEIELSEPDV HGQWKLKGQP LTASPDSEII EDGKKHILIL
 351  HNSQLGMTGE VSFQAANAKS AANLKVKELL IEARALIEVE KPIYGVEVFV
 401  GETAHFEIEL SEPDVHGQWK LKGQPLTASP DSEIIEDGKK HILILHNSQL
 451  GMTGEVSFQA ANAKSAANLK VKELCC
```

Fig. S1 Secondary structure (a) and protein sequence (b) of the $I27_5$ polyprotein used in this study. The molecule comprises five mutated *I*27 domains concatenated with unstructured linker regions (light blue). The secondary structure is predominantly composed of β-sheets (rectangles) and contains 5 tyrosine residues, (ringed by purple circles) which act as crosslink sites

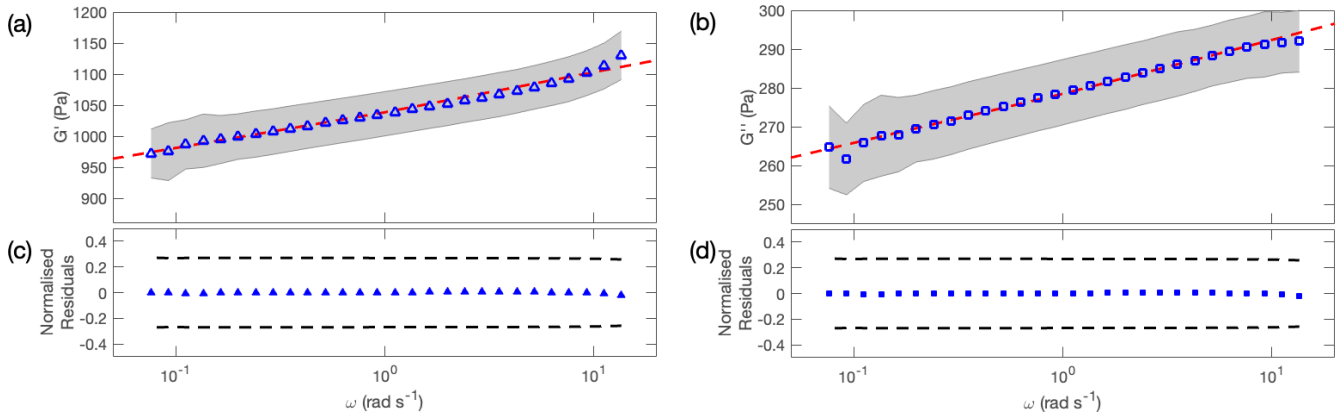

Fig. S2 Mean values of G' (a) and G'' (b) in the linear viscoelastic regime, plotted with linear scaling in the y dimension. The shaded error shows the standard deviation. Dashed lines show the power law fit. Normalised fit residuals for G' (a) and G'' (b) show that all data points (symbols) are comfortably within one standard deviation (dashed lines).

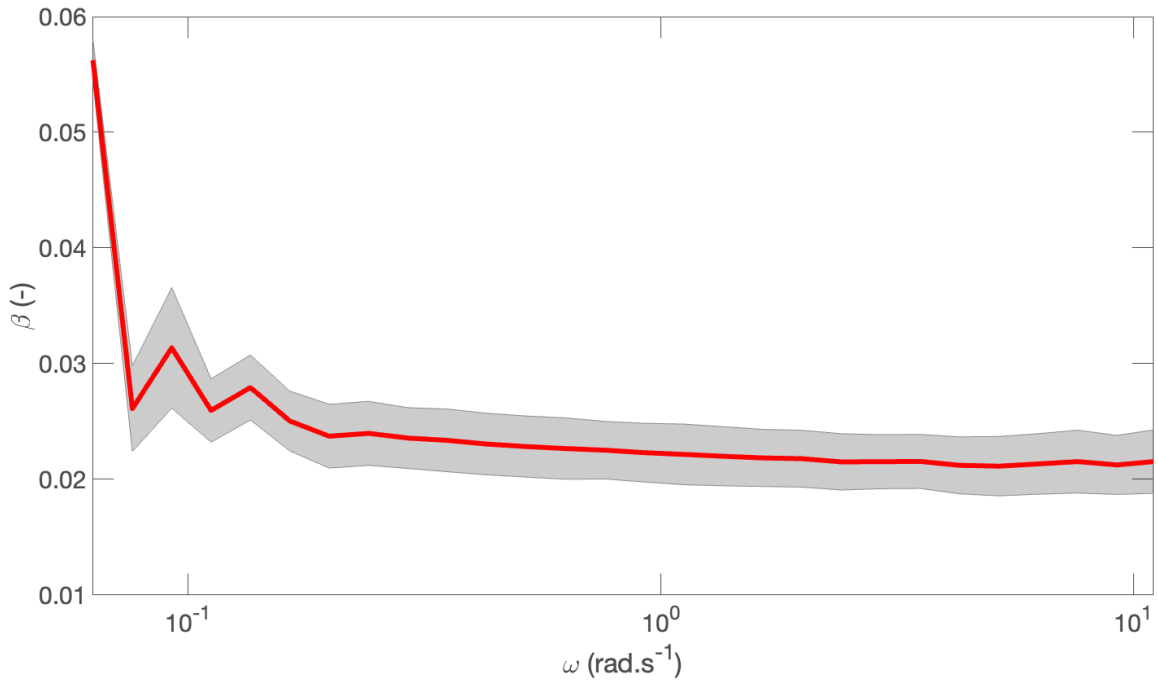

Fig. S3 Power law exponent β as verified independently using the Kramers-Kronig relation of G'' and G'. For $\omega > 1$ rad s^{-1}, β is shown to plateau to an average value of 0.022 ± 0.002, in excellent agreement with power laws fitted to G' in figure 1. Error bars (shaded regions) represent averaged measurements.

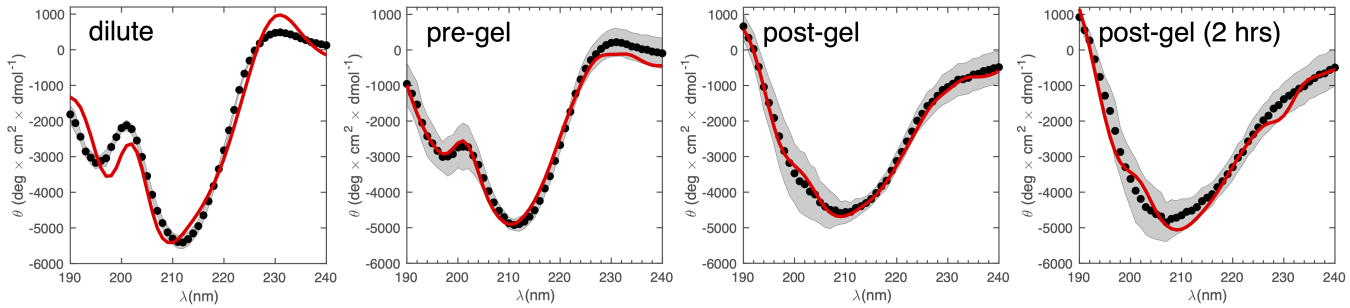

Fig. S4 Best fits (solid red lines) to the mean residue ellipticity of $I27_5$ hydrogels (black circles) at dilute concentrations (5 μM) and at each stage of the gelation process. Fits are carried using the CONTINLL parameter set in Dichroweb. Error bars (shaded regions) represent averaged measurements across different samples.

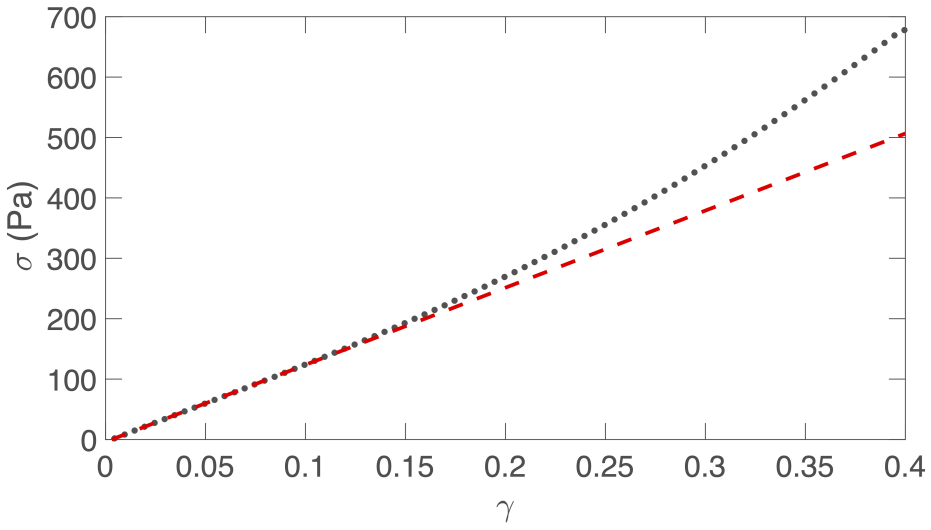

4

Fig. S5 Representative stress-strain Curve of an $I27_5$ hydrogel, captured at a shear strain rate of 0.01 s^{-1} (black dotted line). Excellent agreement with a linear viscoelastic response (red dashed line) is observed for strain $\gamma < 0.1$.

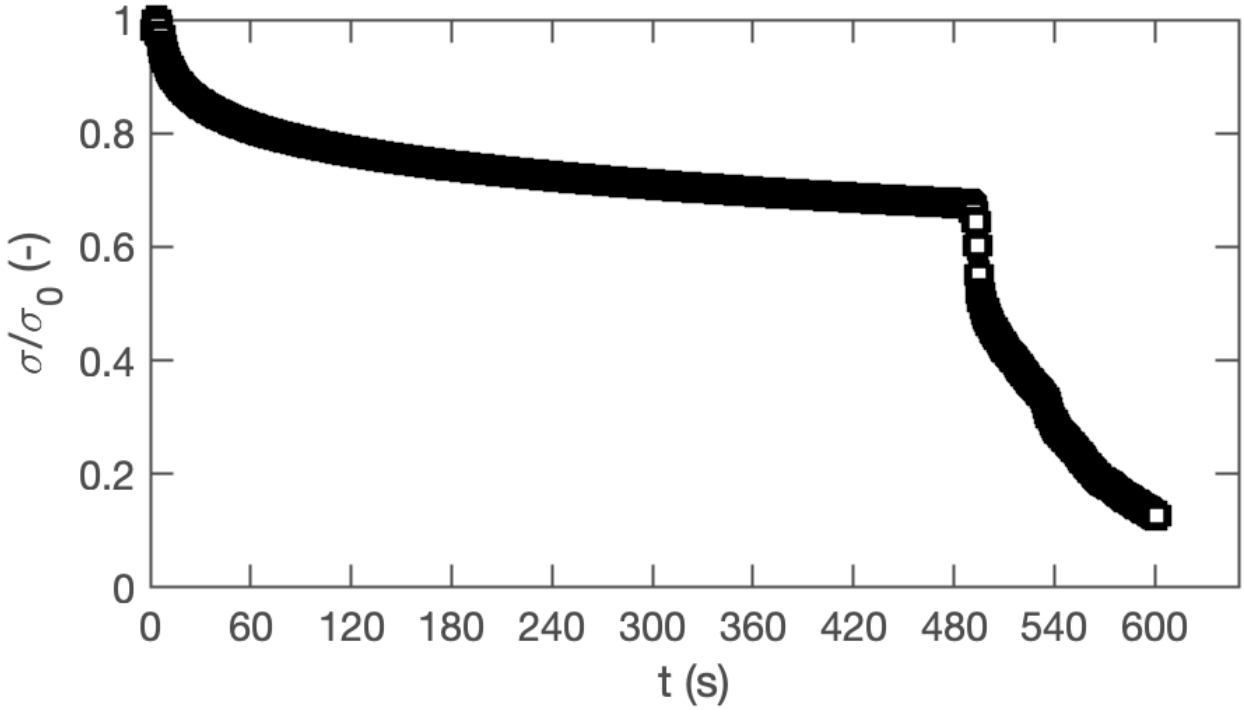

Fig. S6 Representative stress relaxation curve at high step strain ($\gamma = 0.35$). The relaxation curve is discontinuous, indicating that the sample undergoes irreversible failure.

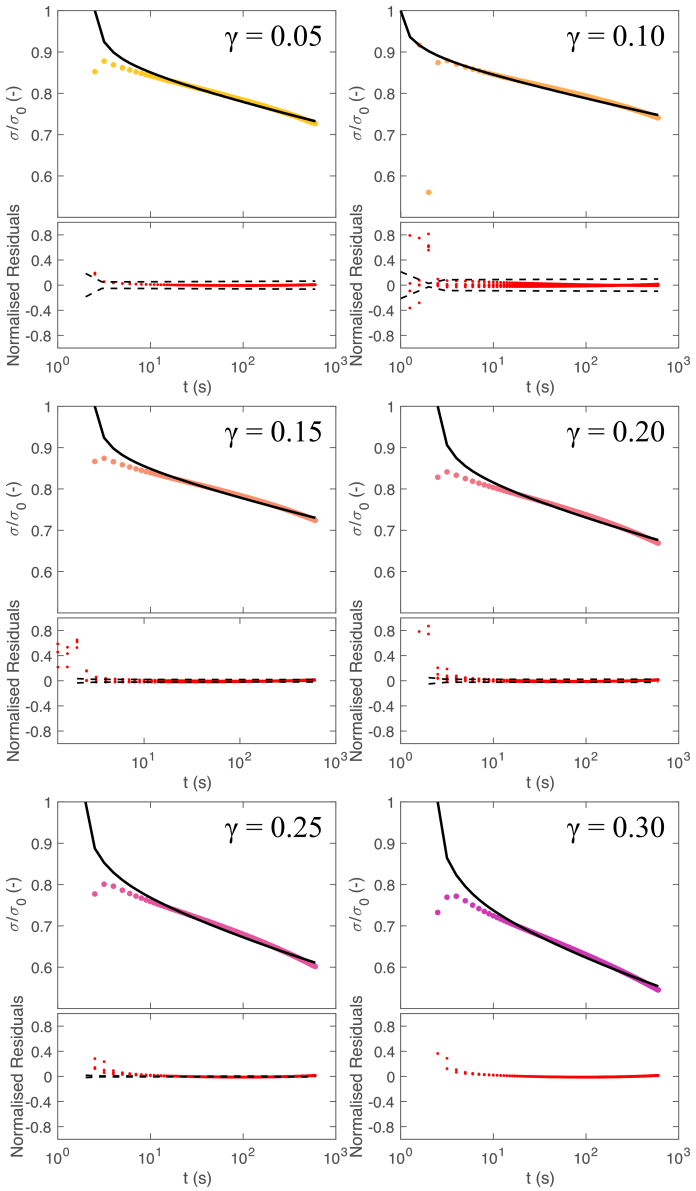

Fig. S7 Normalised relaxation with respect to time t at different values of applied step strain γ, plotted with logarithmic scaling in the x dimension. A springpot model (black lines) provides a close a fit for the data for $t > 5\ s$. Poor fitting at early timescales is likely to be an experimental artifact due to inertial errors associated with reaching a steady state strain. With the exception of these early timescales, normalised residuals are low (lower plots, red circles) in comparison to standard deviation between separate experiments (lower plots, dashed lines). Standard deviations are not shown for $\gamma = 0.30$ since the number of independent samples is insufficient due to the high occurrence of sample failure at high strains.

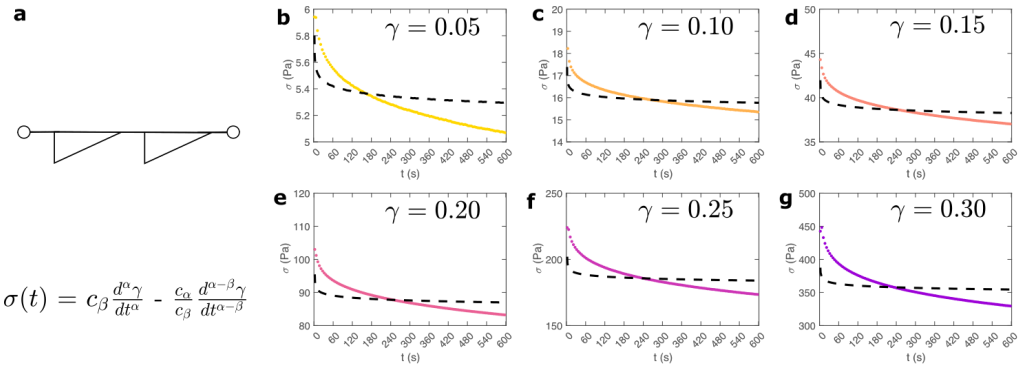

Fig. S8 Best fit of a fractional maxwell model (a) to stress relaxation data at a range of different applied strains. Model fits are shown as dashed lines.

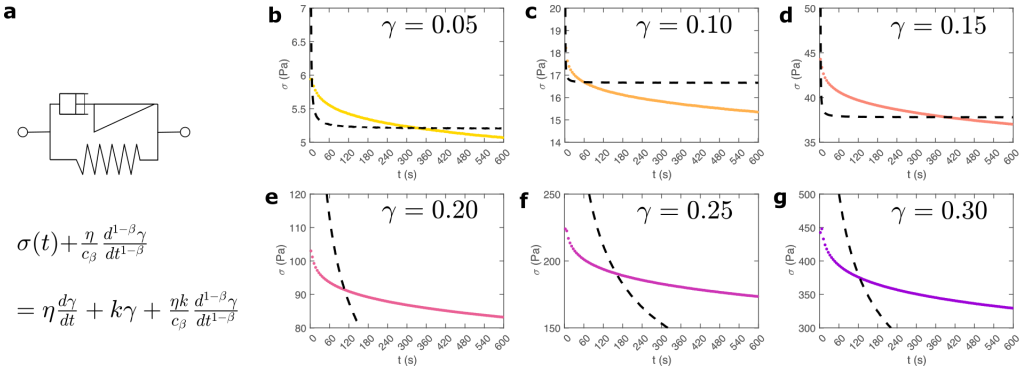

Fig. S9 Best fit of a modified Fractional viscoelastic model comprising a fractional springpot element in series with a spring and in parallel with a dashpot (a). The fit is applied to stress relaxation data at a range of different applied strains (b)-(g). Model fits are shown as dashed lines.

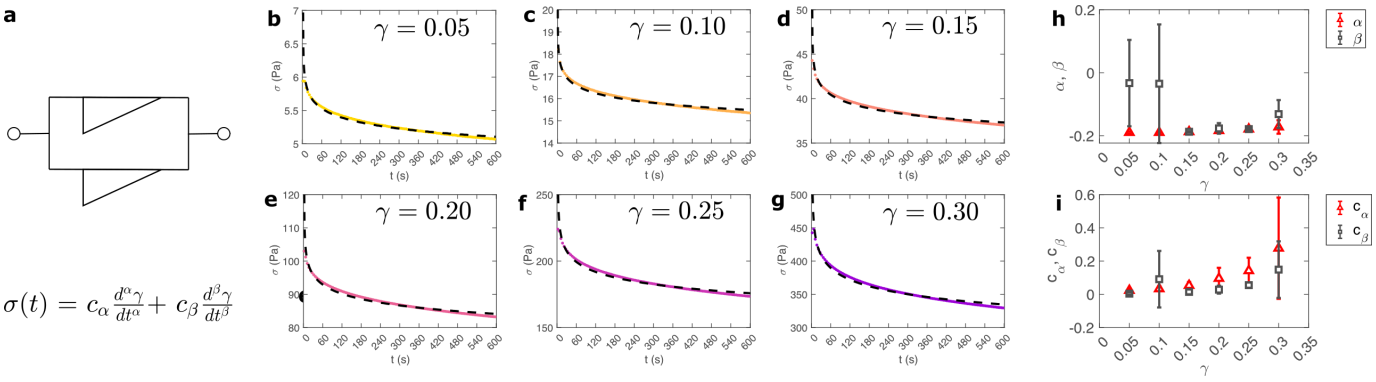

Fig. S10 Best fit of a fractional Kelvin Voigt model comprising two springpot elements in parallel. (a). The fit is applied to stress relaxation data at a range of different applied strains (b)-(g). While the model fits the data closely, the parameters c_α and α are within the error margins of parameters c_β and β (h)-(i) suggesting that additional parameters cause the fitting to become degenerate. Error bars represent averaged measurements across different samples. Model fits are shown as dashed lines.

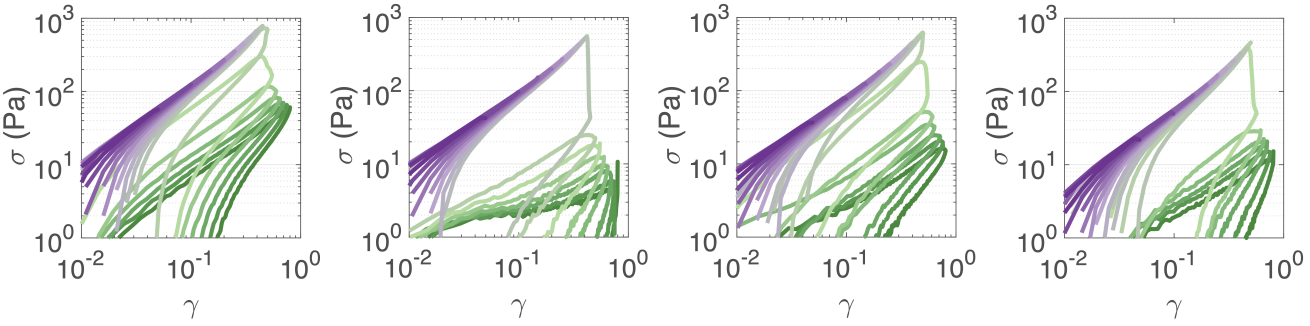

Fig. S11 Representative cyclic loading data showing measured stress with respect to applied strain. Solid lines are loading curves, dashed lines are unloading curves. Colours indicate different loading cycles. Repeat measurements show largely identical nonlinear response, with only slight differences in the network failure point, denoted by a sudden decrease in stress.

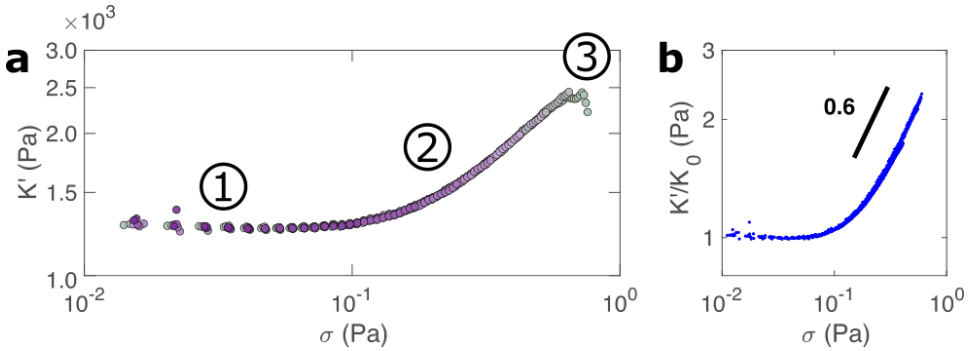

Fig. S12 Differential elastic modulus K' with respect to the sample stress, extracted from multiple loading cycles (a). Colours and regimes of mechanical response (1-3) are equivalent to figure 4. Once K' is normalised to account for slight differences in the linear modulus G_0, data from all repeat measurements superimpose perfectly on to a single curve (b). The hydrogel stiffens as $K' \sim \sigma^{0.6}$.

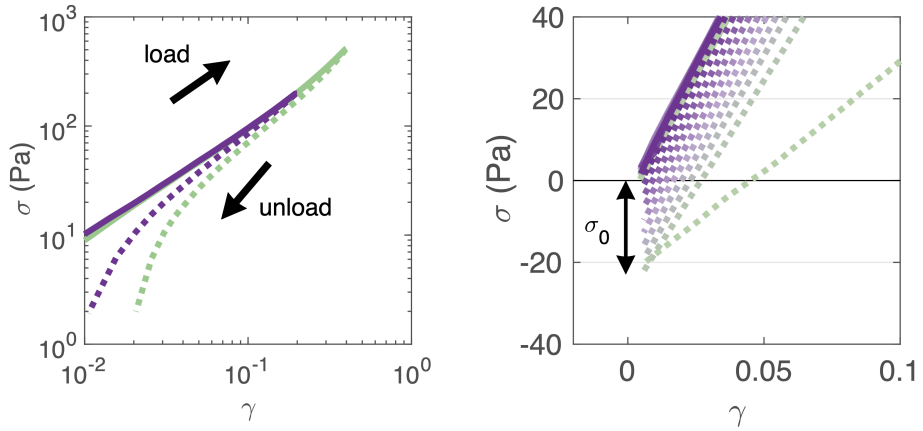

Fig. S13 Definition of the remodelling parameter σ_0. As the network is progressively remodelled after repeated loading cycles, a negative stress σ_0 required to return the network to zero strain. An increase in σ_0 indicates an increase in network remodelling.

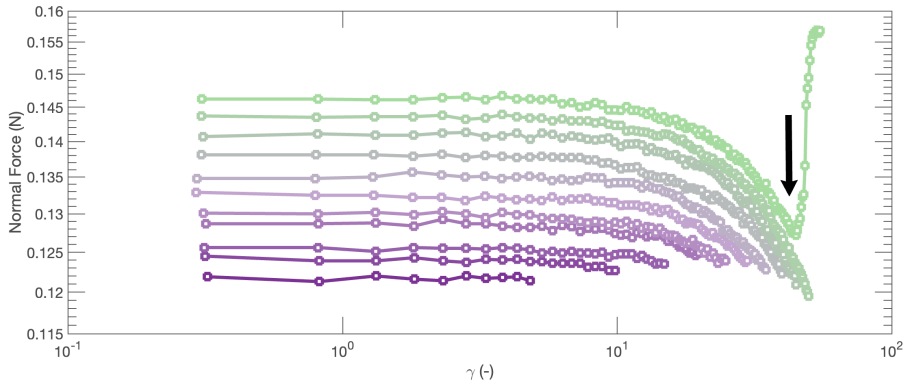

Fig. S14 Evolution of normal force over successive loading cycles. Only loading curve data is shown. During each successive loading cycle, the normal force decreases due to the alignment of the semiflexible protein chains. The gradual increase in normal force after each successive loading cycle is indicative of permanent network remodelling. Network failure is marked by a sharp increase in normal force as shown by arrow. Colours are equivalent to figure 4

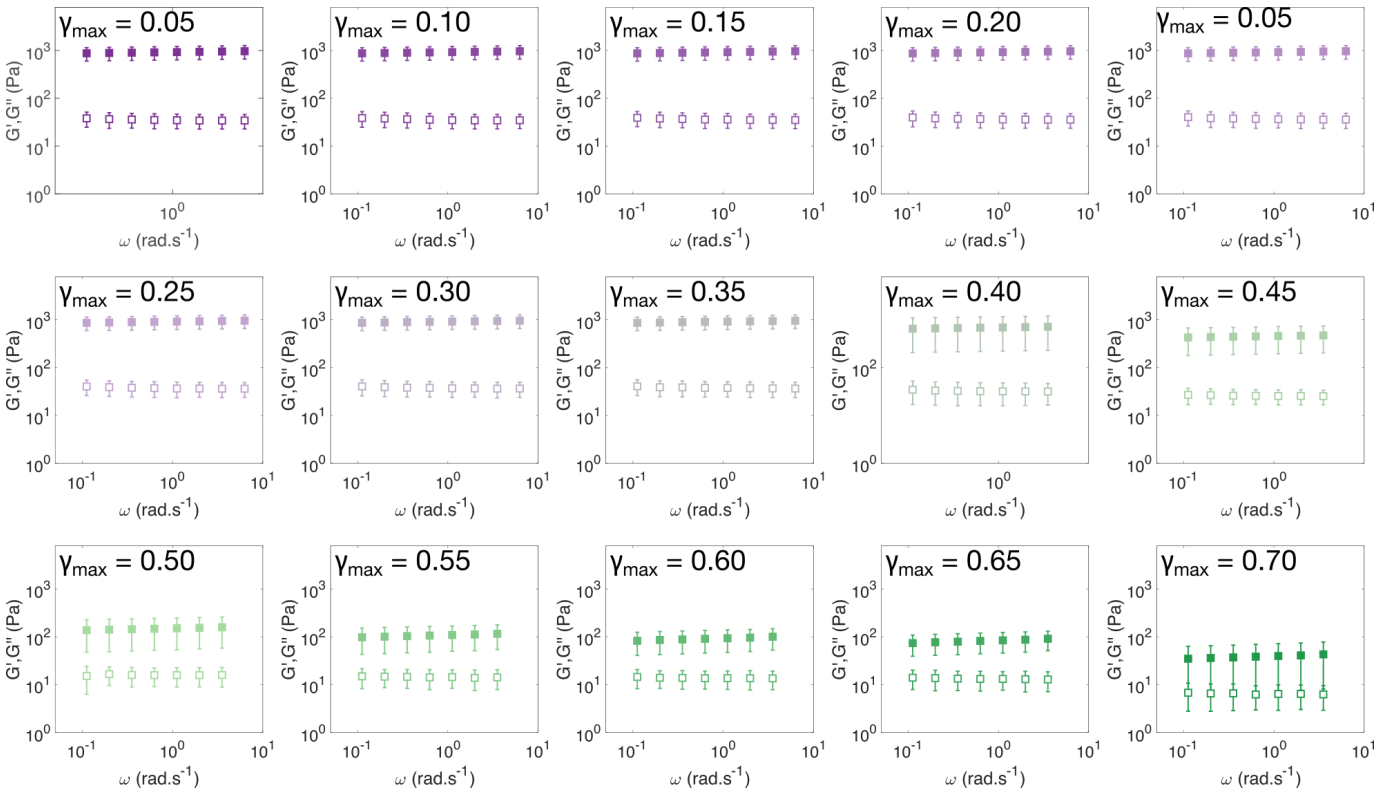

Fig. S15 Representative frequency sweeps of the $I27_5$ hydrogels following the application of triangular strain pulses of increasing magnitude. Each frequency sweep probes the linear viscoelastic properties of the hydrogel after deformation. The spectra remain remarkably consistent at applied strains γ below approximately 0.4, at which point the network undergoes irreversible failure.